

Unconventional photo-induced charge-density-wave dynamics in $2H\text{-NbSe}_2$

R. Venturini,¹ A. Sarkar,¹ P. Sutar,¹ Z. Jagličič,^{2,3} Y. Vaskivskiy,¹ E. Goreshnik,⁴ D. Mihailovic,^{1,5} and T. Mertelj^{1,5,*}

¹*Department of Complex Matter, Jozef Stefan Institute, Jamova 39, 1000 Ljubljana, Slovenia*

²*Faculty of Civil and Geodetic Engineering, University of Ljubljana, Jamova cesta 2, Ljubljana, Slovenia*

³*Institute of Mathematics, Physics and Mechanics, Jadranska 19, Ljubljana, Slovenia*

⁴*Dept. of Inorganic Chemistry and Technology, Jozef Stefan Institute, Jamova 39, 1000 Ljubljana, Slovenia*

⁵*Center of Excellence on Nanoscience and Nanotechnology Nanocenter (CENN Nanocenter), Jamova 39, 1000 Ljubljana, Slovenia*

(Dated: September 6, 2023)

We investigated temperature (T) dependent ultrafast near-infrared (NIR) transient reflectivity dynamics in coexisting superconducting (SC) and charge density wave (CDW) phases of two-dimensional $2H\text{-NbSe}_2$ using NIR and visible excitations. With visible pump-photon excitation (400 nm) we find a slow high-energy quasiparticle relaxation channel which is present in all phases. In the CDW phase, we observe a distinctive transient response component, irrespective of the pump-photon energy. The component is marked by the absence of coherent amplitude mode oscillations and a relatively slow, picosecond rise time, which is different than in most of the typical CDW materials. In the SC phase, another tiny component emerges that is associated with optical suppression of the SC phase.

The transient reflectivity relaxation in the CDW phase is dominated by phonon diffusive processes with an estimated low- T heat diffusion constant anisotropy of ~ 30 .

Strong excitation of the CDW phase reveals a weakly non-thermal CDW order parameter (OP) suppression. Unlike CDW systems with a larger gap, where the optical OP suppression involves only a small fraction of phonon degrees of freedom, the OP suppression in $2H\text{-NbSe}_2$ is characterised by the excitation of a large amount of phonon degrees of freedom and significantly slower dynamics.

I. INTRODUCTION

Layered materials with reduced dimensionality offer a platform for exploring new states of matter. In particular, transition metal dichalcogenides exhibit strong electron-phonon coupling and electron correlations with a rich phase diagram of charge density wave (CDW) phases. These materials have been under intense investigations in recent years as there are many external parameters to control the CDW states, such as hydrostatic pressure¹⁻³, strain^{4,5}, chemical doping⁶, electrostatic doping⁷, and intercalation⁸⁻¹⁰. Recently realized control over these states with optical¹¹ and electrical pulses¹²⁻¹⁴ increased interest in these materials as it opened the way to possible technological applications.

A particularly interesting transition metal dichalcogenide is the $2H\text{-NbSe}_2$ in which an incommensurate 3×3 CDW state forms below $T_{\text{CDW}} = 33\text{ K}$ ¹⁵. The magnitude of the CDW energy gap is up to $\sim 5\text{ meV}$ and is wave-vector dependent¹⁶. Various stripe CDW orders appear with strain⁴, intercalation¹⁷, or after applying an electrical pulse¹⁸. While in many CDW materials, the superconducting (SC) state emerges only after applying pressure^{2,3}, doping¹⁹, or intercalation¹⁰, $2H\text{-NbSe}_2$ is one of the rare examples in which the CDW and superconductivity coexist in a pristine sample. Under high pressure, the CDW is suppressed, while superconducting critical temperature shows an increase¹.

In a typical superconductor, the amplitude (Higgs) mode is not directly observable as it is weakly coupled to electromagnetic fields and is over-damped^{20,21}. In

$2H\text{-NbSe}_2$, however, the coupling between superconductivity and CDW gives rise to a spectroscopically visible SC Higgs mode that has been observed with Raman spectroscopy²²⁻²⁴.

Optical pump excitation with ultrashort laser pulses can both, excite collective modes and give additional information on the nature of electronic states by tracing the single particle and collective mode dynamics. So far, there have been two investigations of $2H\text{-NbSe}_2$ with ultrafast pump-probe spectroscopy.^{25,26} Anikin *et al.*²⁵ investigated $2H\text{-NbSe}_2$ response to a high fluence laser excitation in both normal and superconducting states. Payne *et al.*²⁶ investigated a weaker excitation regime in the CDW state only using a broadband probe. The relatively short timescale data suggested that the decay time of the laser-excited CDW state is diverging around the CDW transition temperature. The critical fluence for the suppression of the CDW state at low- T was estimated to be around $60\text{ }\mu\text{J}/\text{cm}^2$.

The observed transient reflectivity signal from recent pump-probe experiments has, however, proved difficult to interpret as there is a significant fast electron background signal overlapping with the CDW response. Additionally, the transient response of a CDW in $2H\text{-NbSe}_2$ is very long-lived, so a study with longer delay between the pump and probe would be useful to understand the slow dynamics.

We performed all-optical pump-probe experiments at the 1.55 eV pump- and probe-photon energy that was not covered in the previous experiments, and observe a strong charge density wave response with minimal back-

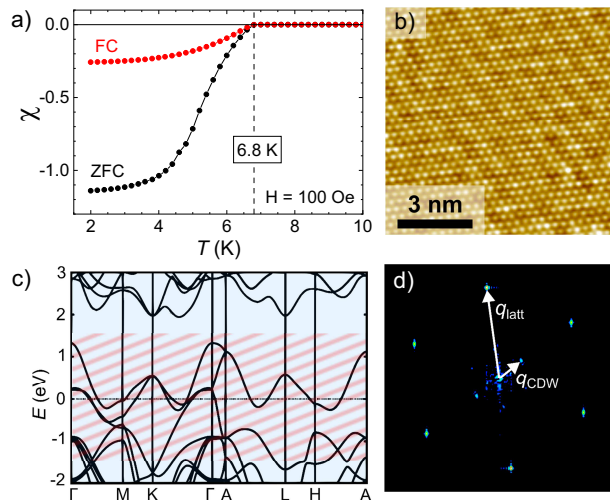


Figure 1. Sample characterization. a) Temperature dependence of the SQUID magnetic susceptibility shows the crystals are superconducting below 6.8 K. b) A 4.2-K scanning tunneling microscope image (set point parameters: tip bias $V = -50$ mV, $I = 160$ pA) and d) the corresponding Fourier transform showing the $\sim 3 \times 3$ CDW state. c) The electronic band structure adapted from Ref. [25]. The red hatched region corresponds to the 1.55 eV photon accessible excitation range. The 3.1 eV photon accessible excitation range exceeds the plotted energy range.

ground. We observe that the CDW state is fragile as it is suppressed at a laser fluence of the order of ~ 10 $\mu\text{J}/\text{cm}^2$ only, depending on the pump photon energy. The suppression is not strongly non-thermal as a large number of phonon degrees of freedom are excited concurrently. For long pump-probe delays we observe that the excited state decay time is fluence- and temperature- dependent, where the dynamics is governed mainly by phonon diffusion processes. We also extend the previous works by using a larger pump-photon energy (3.1 eV) revealing a hitherto unreported high energy quasiparticle bottleneck.

At a very low pump fluence, we observe a transient reflectivity response component due to the superconducting state. Similar to previous pump-probe experiments we do not observe any coherent oscillations that could be attributed to the excitation of the SC Higgs mode, or the CDW amplitude mode.

II. METHODS

A. Sample growth and characterization

$2H\text{-NbSe}_2$ single crystals were synthesized by means of the chemical vapor transport method from stoichiometric amounts of niobium foil and selenium powder with iodine as a transport agent. The material was sealed in a quartz ampule, put into a three-zone tube furnace with

temperature gradient $T_H = 750$ C and $T_L = 680$ C, and slowly cooled to room temperature. Crystal structure and composition were verified with single-crystal X-ray diffraction and energy-dispersion spectroscopy, respectively. We used SQUID measurements to determine the magnetic susceptibility χ . The data show [Fig. 1 a)] that the sample is superconducting below 6.8 K. Additionally we performed an STM characterization of a $2H\text{-NbSe}_2$ cleaved surface at 4.2 K and observed the $\sim 3 \times 3$ charge density wave shown in Fig. 1.

For optical measurements the crystals were exfoliated before mounting into an optical cryostat to obtain a high-quality surface.

B. Transient optical spectroscopy

The 2-pulse and 3-pulse transient reflectivity measurements^{27,28} were performed using 50-fs linearly polarized regenerative amplifier pulses at 800 nm wavelength and the 250 kHz repetition rate. We used the pump (P) pulses at either the laser fundamental ($\hbar\omega = 1.55$ eV) or doubled ($\hbar\omega = 3.1$ eV) photon energy (PE) and the probe (Pr) pulses at $\hbar\omega = 1.55$ eV. In the 3-pulse case we used additional intense driving (D) pulses (also at $\hbar\omega = 1.55$ eV) with a variable delay with respect to the P pulses (see Fig. 3).

Both the 2-pulse and 3-pulse transient reflectivity, $\Delta R/R$ and $\Delta R_3/R$, respectively, were measured by monitoring the intensity of the weak Pr beam. The large direct contribution of the unchopped D beam to the total transient reflectivity, ΔR , was rejected by means of a lock-in synchronized to the chopper that modulated the intensity of the P beam only. Due to the chopping scheme, the measured quantity in the 3-pulse experiments is the difference between the transient reflectivity in the presence of P and D pulses, $\Delta R_{DP}(t_{Pr}, t_P, t_D)$, and the transient reflectivity in the presence of the D pulse only, $\Delta R_D(t_{Pr}, t_D)$:

$$\Delta R_3(t_{Pr}, t_P, t_D) = \Delta R_{DP}(t_{Pr}, t_P, t_D) - \Delta R_D(t_{Pr}, t_D), \quad (1)$$

where t_{Pr} , t_P and t_D correspond to the Pr, P and D pulse arrival times, respectively. In the limit of vanishing D pulse fluence $\Delta R_3/R$ is reduced to the standard two-pulse transient reflectivity $\Delta R/R$.

The P/D and Pr beam diameters were 40-70 and 18-30 μm , respectively. The Pr fluence was ~ 10 $\mu\text{J}/\text{cm}^2$. For the 3-pulse measurements the fluence of the P pulse, $\mathcal{F}_P \lesssim 20$ $\mu\text{J}/\text{cm}^2$, was kept close to the linear response region. The polarizations of the P and D beams were perpendicular to the Pr beam polarization with a random orientation with respect to the crystal axes.

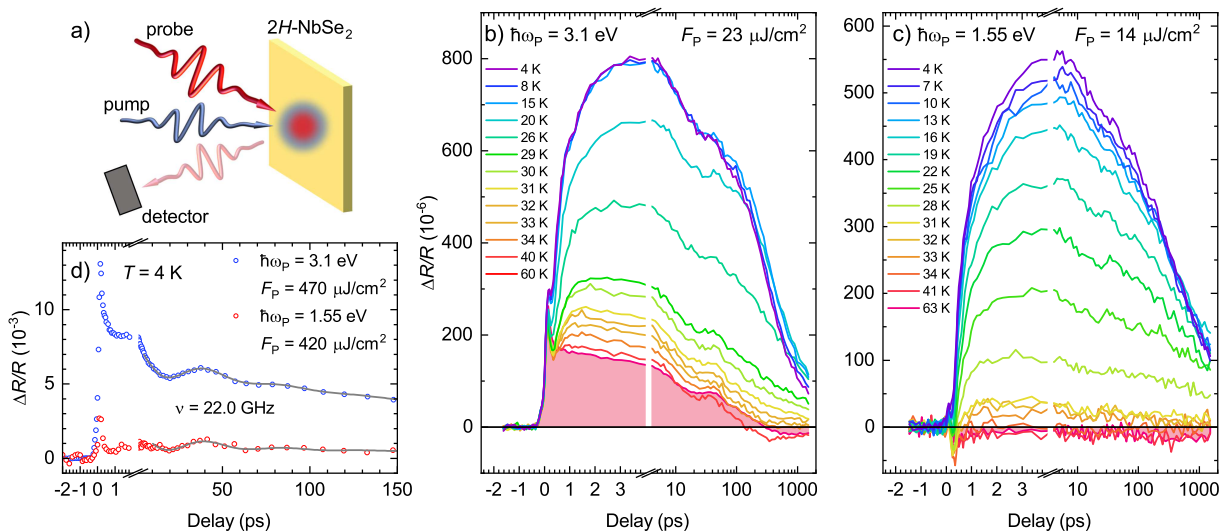


Figure 2. Temperature dependent transient reflectivity. a) Schematics of the 2-pulse pump-probe experiment. b) and c) T -dependent reflectivity transients with 3.1 eV and 1.55 eV pump-photon energy, respectively. Note the logarithmic scale after breaks in b) and c). d) High- F_p transients reveal more clearly the coherent sound wave oscillations. The lines are fits discussed in the text.

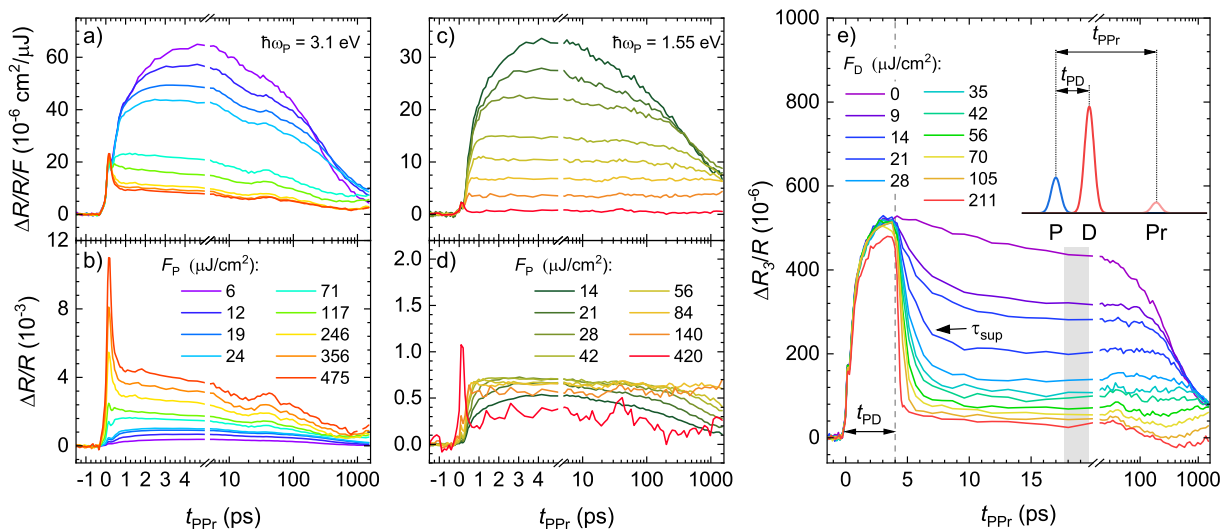


Figure 3. Fluence dependent transient reflectivity at $T = 4 \text{ K}$. a) T -dependent F_p -normalized reflectivity transients at the 3.1 eV pump-photon energy. Note that curve overlap indicates a linear scaling with F_p . b) The corresponding unnormalized transients. c), d) The same at 1.55 eV pump-photon energy, respectively. The increased noise at high F_p is due to the pump scattering. e) 3-pulse transients as a function of the driving-pulse fluence, F_D , at $F_p = 19 \mu\text{J}/\text{cm}^2$. The schematics indicating the pulse sequence is shown in the inset. The shaded region corresponds to the amplitude readout pump-probe delay discussed in the text while the vertical dashed line represents the D-pulse arrival time.

III. RESULTS

In Fig. 2 b) and c) we plot the temperature dependence of the transient reflectivity at 3.1 eV and 1.55 eV pump-photon energies (PPE). At the 3.1 eV PPE [Fig. 2 b)] the normal-state $\Delta R/R$ consists of the initial sub-picosecond component followed by a long-lived, slightly oscillatory, response extending beyond $\sim 100 \text{ ps}$. An additional component with $\sim 1 \text{ ps}$ rise-time and a few hun-

ded ps decay time appears on top of the normal-state response as the temperature is lowered below T_{CDW} . At the 1.55 eV PPE [Fig. 2 c)] we observe a much weaker transient signal above T_{CDW} . Below T_{CDW} , identically to the 3.1 eV PPE case, a long-lived CDW component emerges that slowly saturates in amplitude as the temperature is lowered.

In Fig. 2 d) we show the high- F_p $\Delta R/R$ at both PPE, which more clearly reveals the coherent damped oscilla-

tory part of the response, which is present also in the low- F_P transients. By fitting a damped cosine function (gray curve) we determine the frequency of 22 GHz. The coherent oscillatory component does not show a notable T dependence at any F_P .

Fig. 3 a)-d) shows the low- T F_P -dependent $\Delta R/R$ at both PPE. The CDW component shows saturation with increasing F_P above $\sim 20 \mu\text{J}/\text{cm}^2$. At 3.1 eV PPE the normal-state response, including the oscillatory component, scales linearly with F_P and overwhelms the transients at higher F_P .

With increasing F_P the CDW component saturates and develops a flat-top shape with a rather sharp sub-ps rise, while the relaxation timescale shifts beyond nanosecond timescale. The saturation behavior is associated with a CDW suppression²⁹ by the pump pulse. To study the saturation F_P region avoiding the normal-state background we performed also a 3-pulse experiment²⁸ where another strong driving (D) pulse at 1.55 eV PE is introduced to suppress the CDW independently of the pump pulse. The D pulse is applied at $t_{DP} = 4$ ps, near the temporal maximum of the CDW component. As shown in Fig. 3 (c) we observe a suppression³⁰ of the CDW component on a $\tau_{\text{sup}} \sim 2.5$ ps timescale at low F_D , which decreases with increasing F_D to, $\tau_{\text{sup}} \sim 0.5$ ps, at the complete suppression [see Fig. 3 (e)].

All high F experiments displayed reversible behavior with the maximum F being limited to $\sim 1 \text{ mJ}/\text{cm}^2$.

IV. DISCUSSION

A. Normal state response

We start by discussing the T and F independent coherent oscillatory component that corresponds to the photo-excitation induced sound wave³¹. In order to observe such a wave the real part of the refractive index must be larger than the imaginary part, $n > \kappa$, at the Pr photon energy [see Appendix VI, Eq. (11)]. Calculating the optical constants at the Pr photon energy (1.55 eV) from Dordevic *et al.*³² we obtain the out-of-plane sound group velocity, $c_{sz} = 2540 \pm 70 \text{ m/s}$.³³ On the other hand, taking the literature static elastic constant³⁴, $c_{33} = 46 \text{ GPa}$, we obtain $c_{sz} = 2670 \text{ m/s}$. The $\sim 10\%$ discrepancy can be attributed to the experimental inaccuracy of the refraction index.

Next, we discuss the PPE dependence of the normal state $\Delta R/R$ that is much larger at 3.1 PPE. The band structure of $2H\text{-NbSe}_2$ is characterized by a band gap between the partially occupied bands, with mixed Se- p /Nb- d character extending up to ~ 1.2 eV above the Fermi energy, and, separated by a gap, the Nb- d character dominated bands starting ~ 2 eV above the Fermi energy³⁵ [see Fig. 1 c)]. The photo excitation of the latter is possible only at the 3.1 eV PPE and can contribute to the 1.55 eV $\Delta R/R$ only while they are occupied. The 3.1 eV PPE transient response extending beyond 100 ps

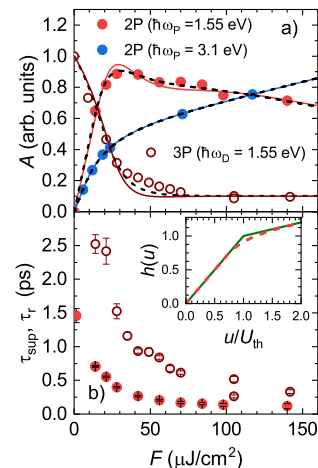


Figure 4. Selected F -dependent transient response parameters at $T = 4$ K. a) The fluence dependence of the signal amplitudes. The open symbols correspond to the 3-pulse experiment. The lines are the saturation model fits discussed in text. b) The rise time (full circles) and 3-pulse signal suppression time (open circles) as function of F . The inset to b) shows the assumed saturation functions discussed in text.

at low F therefore suggests that a slowly-relaxing weakly-coupled electron “pocket” exists in the bands ~ 2 eV above the Fermi energy. This is somewhat unexpected since $2H\text{-NbSe}_2$ is metallic at any T and the Auger relaxation across the band gap is not *a priori* forbidden by energy conservation.

B. CDW and SC state response

We turn first to the CDW component. With decreasing T it appears below T_{CDW} [Fig. 2 b), c)], similar as reported previously using the 1.03 eV Pr photon energy,²⁶ but shows different low- T amplitude saturation. In Ref. [26] it saturates below ~ 25 K, while in the present case, using the 1.55 eV Pr photon energy, it clearly saturates only below $T \sim 15$ K at 3.1 eV PPE [Fig. 2 b)], while at 1.55 eV PPE it does not saturate down to the lowest $T = 4$ K [Fig. 2 c)]. The saturation seems to be connected with the excitation density, which was the lowest, $F_P = 14 \mu\text{J}/\text{cm}^2$, in the present 1.55 eV PPE experiment. We therefore need to discuss the excitation density dependence before continuing to discuss the T dependence.

1. Excitation density dependence in the CDW state

In Fig. 4 a) we summarize the F dependence experiments from Fig. 3 by plotting the magnitudes³⁶ of the transient responses as functions of the relevant fluence for the standard two-pulse 1.55 eV and 3.1 eV PPE experiments as well as the 3-pulse experiment. All the magnitudes show (partial) saturation with increasing F that is

$\hbar\omega$ (eV)	n^a	α^{-1} (nm) ^a	R^a	ϕ	F_{th} ($\mu\text{J}/\text{cm}^2$)	U_{th} (J/cm^3)	T_{th} (K)
3.1 (2-pulse)	3.5	21	0.38		4.5 ± 0.7	1.3 ± 0.2	~ 28
1.55 (2-pulse)	3.2	83	0.3	1.57 ^b	14 ± 0.5	1.2 ± 0.05	~ 26
1.55 (3-pulse)	3.2	83	0.3		19 ± 0.8	1.6 ± 0.07	~ 29

^a Calculated from data in Ref. [32].

^b The phase shift [Eq. (5)] value was fit for the case of the 1.55 eV PPE 2-pulse experiment and taken as a fixed parameter for the 3.1 eV PPE 2-pulse and 3-pulse experiments.

Table I. The CDW destruction threshold fluences, energy densities, estimated peak transient temperatures at F_{th} , and the relevant optical parameters.

attributed to the CDW state suppression²⁹, with an onset around $F \sim 10 \mu\text{J}/\text{cm}^2$. The virtually linear F dependence beyond the saturation region is the consequence of the normal-state background, which scales linearly with F and is the largest in the case of the 3.1 eV PPE.

To extract the absorbed-energy density at the CDW-suppression threshold, U_{th} , we apply the saturation model^{28,37}. In the model we assume a nonlinear transient dielectric function, $\Delta\epsilon$, dependence on the absorbed-energy density, U , at U_{th} [Appendix VI, Eq. (7)]. In addition, we take into account the inherent excitation density inhomogeneity and the optical-probe response kernel²⁸ [Appendix VI, Eq. (4)]. The fits to the F -dependent $\Delta R/R$ magnitudes, derived from the model, as described in detail in Appendix VI, are shown in Fig. 4 a).

The saturation model²⁸ predicts a possibility of oscillatory transient-response-amplitude F dependence, when the probe-PE refraction-index real part, n , exceeds the refraction-index imaginary part, κ , (see Appendix VI and Ref. [28]) due to the interference effect on a thin surface layer, where the CDW order parameter (OP) is optically suppressed. Despite $n/\kappa \approx 4.1$ in $2H\text{-NbSe}_2$,³⁸ we observe no clear oscillatory behavior in the data. This can be partially attributed to the lateral thickness distribution of the suppressed-OP layer due to the Gaussian beam profile and a particular combination of the static and transient dielectric function components [see Eq. (5)] resulting in the kernel shape (see Fig. 5) that minimizes the oscillations.

In the case of the 1.55 eV PPE 2-pulse experiment, however, the model oscillations can not be completely washed out by the above mentioned effects effects, as indicated by the red curve in Fig. 4 a). Assuming some smearing in the nonlinear local dielectric function U -dependence around U_{th} [see Eq. (7) and insert to Fig. 4 b)] leads to virtually complete suppression of the oscillations as indicated by the black dashed lines in Fig. 4 d). The smearing suggests an absence of a sharp boundary between the suppressed and non-suppressed OP regions which is plausible due to presence of a strong transient chemical potential gradient, causing quasiparticle and possibly CDW-sliding currents between the regions.

The application of smearing does not significantly affect the obtained U_{th} so the values from the fits in the absence of the smearing are reported in Tab. I. Focusing first on the 2-pulse experiments, U_{th} is found somewhat

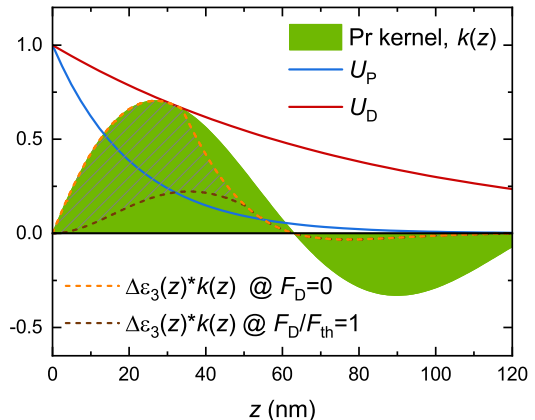


Figure 5. Depth dependence of the probe kernel [Eq. (4)] in comparison to the normalized P and D deposited energy density profiles. The model kernel-weighted 3-pulse response [Eq. (8)] at two selected D fluences is also shown with the dashed lines. The hatched region corresponds to the 3-pulse signal suppression profile at $F_{\text{D}} = F_{\text{th}}$. The kernel parameters were taken from Tab. I. The phase shift, $\phi \sim \pi/2$, obtained from the fit is such, that the negative-sign kernel region is relatively deep in the sample, minimizing its contribution to the signal.

larger at the 3.1 eV PPE, but the difference is within the fitting error bars. Using the heat capacity data³⁹ we estimate the enthalpy change when heating the sample thermally to T_{CDW} to be, $\Delta H_{\text{CDW}} \approx 2.5 \text{ J}/\text{cm}^3$. The experimental U_{th} values around a half of ΔH_{CDW} therefore indicate that the CDW suppression is non thermal, however, due to the small low- T phonon specific heat capacity the peak transient temperature, T_{th} , corresponding to the fully thermalized excitation volume is relatively large, above $\sim 26 \text{ K}$ at U_{th} (see Tab. I).

Applying the saturation model to the 3-pulse experiment (Eq. 8) results in a larger U_{th} and the fit departs from the data at higher F_{D} [see Fig. 4 a)] even when assuming the smearing (see the dashed fit curve). To understand this one has to take into account important differences between the 2-pulse and 3-pulse experiments. (i) At the used experimental parameters, the 3.1 eV PE P pulse, with $F_{\text{P}}/F_{\text{th}} \sim 5$, suppresses the CDW within the depth, $z_{\text{P}} \sim 34 \text{ nm}$, before the arrival of the D pulse. (ii) The measured ΔR_3 is referenced to ΔR_{D} , obtained in the presence of the D-pulse only [Eq. (1)]. (iii) The

ΔR_3 amplitude is read out ~ 14 ps (~ 18 ps) after the D (P) pulse arrival [the gray band in Fig. 3 e)].

Due to (i), (ii) and Eq. (8) the 3-pulse signal at any F_D depends on the detailed behavior of $\Delta\epsilon$ near the saturation threshold as most of the signal comes from the P-suppressed region (see also Fig. 5). Moreover, due to (iii) most likely some thermalization already takes place at the readout t_{PPR} . The measured 3-pulse saturation therefore corresponds to the properties of a partially thermalized strongly excited material even at low F_D , which cannot be taken into account by the present simple model.

Comparing to superconductors and, in particular, to the large-gap CDWs²⁹, a significantly larger amount of the absorbed energy is lost to the phonon bath. In the large-gap CDWs, where the gap energy, 2Δ , exceeds the maximum phonon energy, the phonons do not appear to be strongly involved in the OP suppression at all.²⁹ U_{th} is comparable to the CDW condensation energy and the suppression is highly non-thermal irrespective to the presence of ungapped Fermi surface. This suggests that the initial high-energy photo-excited quasiparticle relaxation is dominated by Auger processes that excite the quasiparticles across the CDW gap, and the CDW is suppressed before the energy is transferred to phonons.

In superconductors, where 2Δ falls within the phonon energy spectrum, it was argued²⁹ that the initial high-energy photo-excited quasiparticle relaxation must be dominated by phonons since the data indicate that most of the absorbed optical energy is lost to the sub-gap phonons that cannot contribute to the pair breaking, and consequently to the superconducting OP suppression. Despite this, U_{th} is found much smaller than the enthalpy change when heating the sample thermally to T_c , so the phonon population must remain highly non-thermal on the picosecond suppression timescale.

In $2H$ -NbSe₂, the CDW gap is in the $\sim 1 - 6$ meV range on the K pockets with negligible/zero CDW gap on the Γ pockets¹⁶ while the phonon spectrum extends to⁴⁰ ~ 30 meV. The energy scales are therefore somewhat similar to the lower- T_c cuprate superconductors²⁹. The relative amount of the gapless electronic density of states is, however, larger in the present case⁴¹ and might be instrumental in transferring the absorbed optical energy to the sub-gap-energy degrees of freedom that are inefficient for the CDW suppression. The ungapped inner-most Γ pocket, which shows strong coupling to the highest energy phonons,¹⁶ stands out in particular, as a possible relaxation channel that bypasses the energy relaxation through the CDW-gapped Fermi surface regions.

The CDW OP suppression times behave quite differently in the 2-pulse and 3-pulse experiments. The 2-pulse transient reflectivity onset in CDWs is often dominated by the coherent amplitude mode (AM) and phonon excitation^{11,42-46} with the rise time of $\sim 1/4$ of the AM period. The low- T AM mode frequency in $2H$ -NbSe₂ is⁴⁷ ~ 40 cm⁻¹ so the corresponding, $\tau_r \sim 0.2$ ps, rise time would be much shorter than the present low- F data with,

$\tau_r \sim 1.5$ ps, show.

The behavior is therefore more similar to the case of the conventional and low- T_c cuprate superconductors^{37,48-50} where the low-excitation-density quasiparticle population evolves according to the Rothwarf-Taylor^{51,52} bottleneck model, with the non-equilibrium-phonons dominated^{48,49} initial conditions. In such case the rise time is in a picoseconds range and it drops with the excitation density, as in the present case.

The CDW state in $2H$ -NbSe₂ is, however, not fully gaped and the bottleneck⁵² is rather weak, as indicated by the relatively large U_{th} . While the slow rise-time timescale suggests the non-equilibrium-phonons dominated suppression it is not clear whether the plain Rothwarf-Taylor model is applicable to explain the weak-excitation⁵³ rise-time behavior in the present case. Nevertheless, the CDW gap on the K pockets seem to somehow avoid fast suppression during the initial photo-excited carrier relaxation suggesting that the dominant high-energy relaxation involves mostly phonons and the L-pockets quasiparticles.

Compared to the 2-pulse experiment, the 3-pulse experiment CDW OP suppression time [Fig. 4 b)] is significantly longer. As discussed above, the 3-pulse signal at any F_D reflects the properties of the highly-excited and strongly-suppressed CDW-OP region, where a critical slowing down of the dynamics might take place. However, the 2-pulse data do not show any critical slowing-down of the rise time near T_{CDW} ruling out the hypothesis, unless the highly excited state phase transition fundamentally differs from the thermal one.

The slower 3-pulse suppression dynamics therefore remains puzzling. A possible origin of such dynamics could be formation of a spatially inhomogeneous OP fluctuating state near F_{th} , consistent also with the absence of the $\Delta R/R$ amplitude oscillations in the 2-pulse F -dependence.

2. Signatures of the SC state

For both 1.55 eV and 3.1 eV PPE, the transient reflectivity with F_P of tens of $\mu\text{J}/\text{cm}^2$, does not show any appreciable change of signal in the SC state below $T \sim 7$ K. However, reducing the fluence to an extremely low value, $F_P = 1.4 \mu\text{J}/\text{cm}^2$, a slight drop in the amplitude is observed when entering the superconducting state below $T_c = 6.8$ K [Fig. 6 a), b)]. The magnitude of the drop is rather small, and is comparable to the signal noise level [Fig. 6 b)]. There is also a tiny difference between the CDW and SC-CDW transients at the longest delays suggesting the presence of a tiny negative long-lived SC component. The absence of any SC state signature at $F_P = 14 \mu\text{J}/\text{cm}^2$ response indicates that the SC induced contribution is already saturated at $F_P = 1.4 \mu\text{J}/\text{cm}^2$. Indeed, the low- T heat capacity is so small that the excited volume transient T exceeds T_c already around

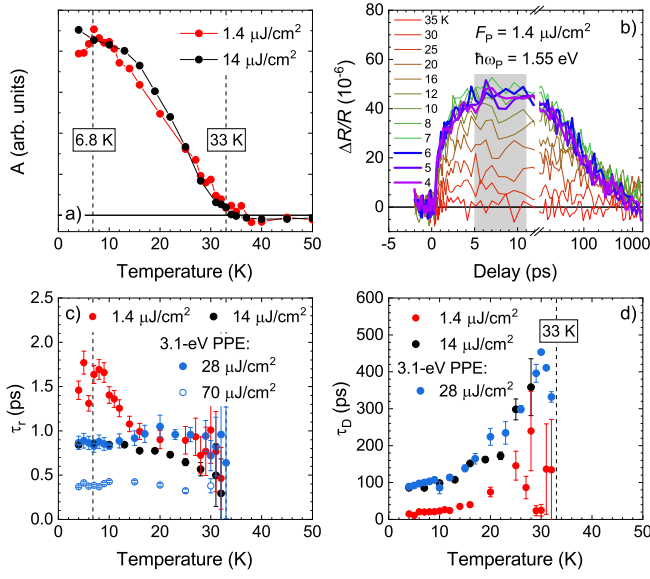


Figure 6. Selected T -dependent transient response parameters. a) The normalized transient reflectivity amplitude as a function of T at two excitation fluences at 1.55 eV pump photon energy. b) T dependence of the lowest pump-fluence transient reflectivity. The shaded region corresponds to the averaging region of the amplitude readout. c) and d) the rise time and relaxation time as a function of T , respectively.

$F_P = 0.5 \mu\text{J}/\text{cm}^2$ at 1.55 eV PPE. The possible observation of the optically coherently excited SC Higgs mode is therefore hindered by the noise level of the present experiment.

3. CDW state temporal dynamics

For discussing the temporal dynamics of the CDW transient reflectivity component we mostly focus on the 1.55 eV PPE data, where the normal-state response is negligible and the rise and decay times can be more reliably quantitatively extracted by simple few parameter fits. A similar analysis is presented also for the 3.1 eV PPE data. However, in addition to the larger normal-state response obscuring the CDW dynamics, most of the 3.1 eV PPE data correspond to the nonlinear response region because the laser fluences used were larger and the optical penetration depth, α^{-1} , is ~ 4 times shorter at the 3.1 eV PPE (see Tab. I) than at the 1.55 eV PPE.

To remove the oscillatory acoustic component contribution (and the large normal-state response in the 3.1 eV PPE case) we subtract the normal state $\Delta R/R$ just above T_{CDW} before fitting to obtain the CDW (+ SC) component shown in Fig. 7 together with different fits discussed below.

We note that the start of the rise of the CDW component in Fig. 7 appears delayed for ~ 200 fs with respect to the pump pulse as can be the most clearly seen in Fig. 3 d). This delay can be attributed to the initial relax-

ation of the high-energy quasiparticles by Auger and/or phonon emission processes.

While the CDW component rise time dynamics can be described reasonably, but not to the finest details, using a single exponential function, the decay dynamics is not exponential (see dotted lines in Fig. 7). It turns out that the 1.55 eV PPE data can be described by a simple three parameter function assuming a diffusive decay:

$$\Delta R/R = A \left[1/\sqrt{1+t/\tau_D} - \exp(-t/\tau_r) \right], \quad (2)$$

in the full CDW temperature range. The first term in the brackets corresponds to a simplified 1D diffusion dynamics⁵⁴, where the characteristic diffusion time, $\tau_D = z_0^2/4D$, corresponds to the optical penetration depth, $z_0 \sim \alpha^{-1}$, diffusion length-scale. The second term describes the rise time dynamics.

The slight discrepancy of the diffusive-decay fit at long timescales at the lowest T and 1.55 PPE can be attributed to the T -dependence of the diffusion constant and the presence of the additional SC component. The much more prominent diffusive-decay fit failure [see Fig. 7 c)] at 3.1 eV PPE, where the exponential decay⁵⁵ fits are somewhat better, however, cannot be of the same origin.

The $\Delta R/R$ decay dynamics at the 3.1 PPE could be affected by the factor of ~ 4 smaller⁵⁶ pump optical penetration depth, resulting in the larger inhomogeneity within the probed volume, and the strong nonlinearity due to the higher excitation density. In Fig. 7 c) we therefore plot also fits (dashed lines) obtained in the framework of the saturation model (see Appendix VI) taking into account a simplified 1D diffusion depth profile (9) and the nonlinearity (7) at U_{th} . Unfortunately, the advanced diffusion model results in a very poor fit at the tens-of-picoseconds timescale.⁵⁷ In the model the CDW OP suppression is expected to spread deeper into the sample, initially, leading⁵⁸ to the transient reflectivity increase on tens-of-picoseconds timescale due to the short 3.1 eV PE pump optical penetration depth and the relatively deeper sensitivity of the probe kernel (Fig. 5). The absence of such a peak in the data therefore suggests an initial fast (a few-picosecond) spread of the excitation beyond the optical penetration depth or/and thermalization of the excited degrees of freedom to the phonon heat bath on a ~ 10 ps timescale, which are not included in the saturation-model diffusion fits.

Moreover, due to a complete CDW OP suppression, formation of topological defects cannot be excluded.^{59,60} This effect should slow-down the recovery and can influence the shape of the transients on several tens⁵⁹ of picoseconds. Due to the similarity of the timescales it is unfortunately not possible to disentangle these effects in the current data.

The characteristic diffusion time, τ_D , obtained from the fits is strongly F_P dependent [Fig. 6 d)], increasing with increasing fluence from ~ 10 ps at the lowest $F_P =$

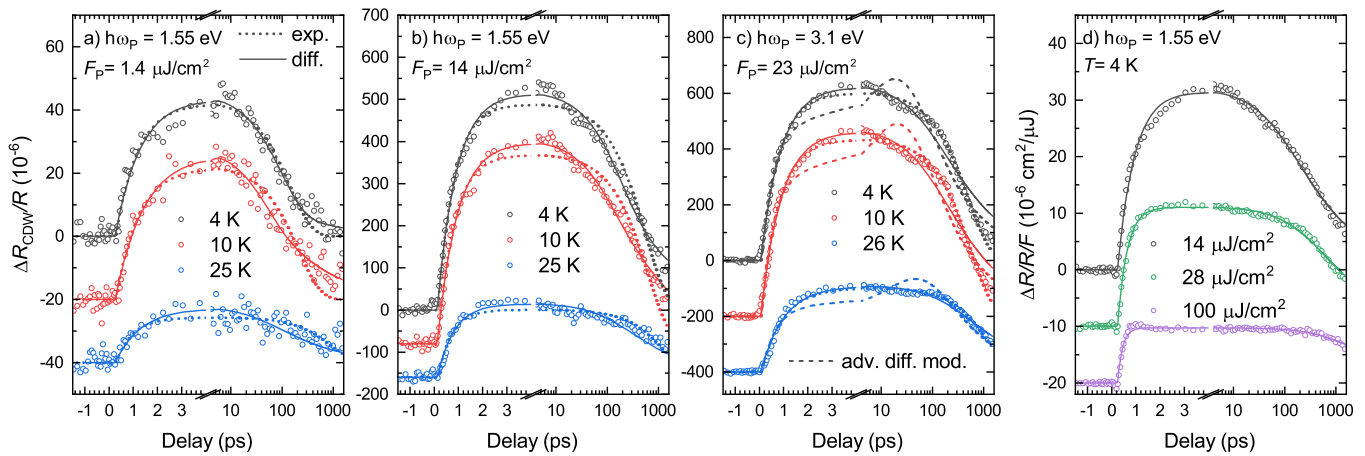


Figure 7. Examples of fits to the data at different excitation conditions. The lines correspond to various decay models discussed in text.

$1.4 \mu\text{J}/\text{cm}^2$ to ~ 90 ps at $F_P = 14 \mu\text{J}/\text{cm}^2$ at the lowest T . The increase of τ_D with increasing F can be attributed to the increased transient T resulting in a decrease of the diffusion constant.

The low- T weak-excitation out-of-plane diffusion constant, $D_{\text{op}} \sim 1 \text{ cm}^2/\text{s}$, obtained from τ_D , appears ~ 30 times smaller than the equilibrium in-plane thermal diffusion constant, $D_{\text{eq-ip}}$.^{61,62} Taking into account that $\sim 1/3$ of the in-plane thermal conductivity in $2H\text{-NbSe}_2$ is due to phonons at low T ,⁶³ this anisotropy is compatible with the rather large resistivity anisotropy^{64,65} of at least several hundred, if the phonon thermal conductivity is less anisotropic. With $\sim 1/3$ of in-plane heat transfer due to phonons the equilibrium thermal diffusion constant anisotropy of $D_{\text{eq-ip}}/D_{\text{eq-op}} \sim 10$ would be consistent with the data.

Since the relaxation appears diffusion dominated it is unclear whether the increase of τ_D with increasing T reflects also a slowing down of the non-equilibrium OP relaxation/thermalization. In the framework of the phenomenological CDW dynamics model by Schaefer *et al.*⁶⁶ the absence of the electronic-mode critical slowing down at T_{CDW} would suggest the adiabatic dynamics, where the electronic OP instantly follows the lattice motion. In this limit a strong softening of the oscillatory AM is expected.⁶⁶ Such mode has not been observed in the 1.55 eV probe PE transient reflectivity, presumably due to a low Raman cross-section and/or inefficient coherent excitation^{67,68} The Raman data⁴⁷, however, indicate a moderate softening of the low- T 40-cm^{-1} A_{1g} Raman mode by $\sim 10 \text{ cm}^{-1}$ and rather large broadening from $\gamma \sim 20 \text{ cm}^{-1}$ at low T to $\gamma \sim 60 \text{ cm}^{-1}$ near T_{CDW} , which suggests the non-adiabatic electronic order parameter dynamics,⁶⁶ where a critical slowing down of the electronic mode is expected.

The likely absence of the slowing down in our data suggests that the Schaefer *et al.*⁶⁶ model is not applicable in the present case. The reason might be the neglecting of the CDW-coupled lattice-mode damping in the model

that might not be fulfilled in $2H\text{-NbSe}_2$ due to the presence of the gapless Γ -pockets Fermi surface.

Focusing again to the rise-time dynamics we plot in Fig. 6 c) the T -dependence of the rise time at different excitation conditions. The lowest- F_P 1.55 eV PPE rise time is found T independent ($\tau_r \sim 1.7$ ps) up to $T \sim 10$ K with a pronounced drop with increasing T beyond ~ 10 K [see Fig. 6 c)] to $\tau_r \sim 1$ ps at $T \sim 15$ K dropping further to $\tau_r \sim 0.8$ ps near T_{CDW} . The rise time drop with increasing F_P [see Fig. 4 b)] appears less pronounced at higher temperatures for the 1.55-PPE case. The behavior is qualitatively consistent with the the non-equilibrium-phonons dominated Rothwarf-Taylor pre-bottleneck dynamics⁵² discussed above.

There is a pronounced difference in the rise time behavior at 3.1 eV PPE, showing T -independent and slightly larger values⁶⁹ consistent with different rate-limiting T -independent and slower high-energy quasiparticle relaxation pathways present at 3.1 eV PPE.

V. SUMMARY AND CONCLUSIONS

The coexisting CDW and SC phases in $2H\text{-NbSe}_2$ were investigated by means of the narrow-band all-optical pump-probe spectroscopy extending the parameter ranges of the previous similar works.^{25,26}

Using 3.1 eV pump photon energy we reveal an unexpected high-energy quasiparticle bottleneck due to a band gap in the unoccupied band manifold which is present at all temperatures.

A systematic fluence dependence transient-reflectivity study shows that the optical CDW suppression, with the absorbed energy density threshold of $\sim 1.2 \text{ J}/\text{cm}^3$ (at $T = 4$ K), is only weakly non-thermal with a large amount of phonons excited concurrently. This is different to the most of the common large-gap CDW materials and superconductors. The low-fluence rise time dynamics data suggest that the CDW suppression path-

way is through hot phonons, similarly to the conventional SCs^{48,49}. The behavior is tentatively attributed to the presence of a relatively large gapless Fermi-surface regions that enable efficient quasiparticle-energy relaxation, without significant quasiparticle excitation in the CDW-gapped hot spots.

To the best of our knowledge, we observe for the first time the concurrent transient responses of the SC and CDW phases. However, only a very weak signature of the SC state was observed, which did not allow for a detailed SC state temporal dynamics analysis.

The CDW state relaxation is found to be dominated by the out-of plane phonon diffusion processes. The heat transport is found to be much less anisotropic than the charge transport, with the estimated low-temperature out-of-plane thermal conductivity ~ 30 times smaller than the in-plane one.

The non-equilibrium-quasiparticle and the CDW order-parameter thermalization-timescale slowing near T_{CDW} ^{26,66} appears unlikely, as most of the slowing down

can be attributed to the T dependence of the diffusion constant.

ACKNOWLEDGMENTS

The authors acknowledge the financial support of Slovenian Research and Innovation Agency (research core funding No-P1-0040 and young researcher funding No. PR-10496). We would also like to thank V. V. Kabanov for fruitful discussions.

VI. SATURATION MODEL

Assuming laterally uniform beams and relatively narrow-band optical pulses the transient reflectivity is given²⁸ by:

$$\frac{\Delta R}{R} = \frac{4\omega_{\text{pr}}}{c_0 |\mathcal{N}^2 - 1|} \int_0^\infty dz e^{-\alpha z} \left[\Delta\epsilon_r(z) \sin\left(2n \frac{\omega_{\text{pr}}}{c_0} z - \beta\right) + \Delta\epsilon_i(z) \cos\left(2n \frac{\omega_{\text{pr}}}{c_0} z - \beta\right) \right], \quad (3)$$

$$\mathcal{N} = n + i\kappa, \quad \tan(\beta) = \frac{2n\kappa}{n^2 - \kappa^2 - 1}.$$

Here n and κ are the static refraction-index real and imaginary parts at the probe PE, $\hbar\omega_{\text{pr}}$, respectively, $\alpha = 2\kappa \frac{\omega_{\text{pr}}}{c_0}$, the probe extinction coefficient and c_0 the vacuum speed of light. $\Delta\epsilon_r(z)$ and $\Delta\epsilon_i(z)$ correspond

to the real and imaginary part of the photo-excitation-induced dielectric function change, respectively.

Assuming, that $\Delta\epsilon_r(z)$ and $\Delta\epsilon_i(z)$ have the same z dependence, $\Delta\epsilon(z) = \Delta\epsilon_0 g(z)$, Eq. (3) is simplified to:, Eq. (3) is simplified to:

$$\frac{\Delta R}{R} = \frac{4\omega_{\text{pr}} |\Delta\epsilon_0|}{c_0 |\mathcal{N}^2 - 1|} \int_0^\infty dz e^{-\alpha z} \cos\left(2n \frac{\omega_{\text{pr}}}{c_0} z - \phi\right) g(z), \quad (4)$$

$$\tan(\phi) = \frac{2n\kappa\Delta\epsilon_{0r} - (n^2 - \kappa^2 - 1)\Delta\epsilon_{0i}}{2n\kappa\Delta\epsilon_{0i} + (n^2 - \kappa^2 - 1)\Delta\epsilon_{0r}}. \quad (5)$$

In addition to the probe n and α (κ), which are given by the static optical properties, the integral kernel depends on the phase shift ϕ . The phase shift strongly influences the kernel shape and, as a result, the depth sensitivity of the probe. It cannot be determined from the static optical constants only and needs to be determined from the transient data.

In the case of coaxial Gaussian beams with finite diameters (4) can be easily extended by an additional integration in the radial direction⁷⁰ where $g(r, z)$ is obtained from an appropriate effective model³⁷ by taking into account the excitation fluence spatial dependence, where r corresponds to the radial distance from the beams center.

In the case of a linear excitation fluence response and a single excitation P beam one can assume,

$$g(r, z) \propto \Delta\epsilon(r, z) \propto U(r, z),$$

$$U(r, z) = F_P(1 - R_P)\alpha_P \exp[-\alpha_P z - 2r^2/\rho_P^2], \quad (6)$$

where $U(r, z)$ is the absorbed energy density. R_P , α_P and ρ_P^2 are the reflectivity, extinction coefficient and diameter of the P beam, respectively.

To take into account suppression of the CDW resulting in a nonlinear $\Delta\epsilon$ excitation dependence we assume a simple phenomenological saturation model²⁸ where we approximate the local amplitude of the transient dielectric function change, $\Delta\epsilon(r, z)$, by a piece-wise linear func-

tion of the locally absorbed energy density, $U(r, z)$, that has different slopes below and above U_{th} :

$$\Delta\epsilon(r, z) = \Delta\epsilon_0 h(U(r, z)),$$

$$h(u) = \begin{cases} \frac{u}{U_{\text{th}}}; & u < U_{\text{th}} \\ 1 + a(\frac{u}{U_{\text{th}}} - 1); & u \geq U_{\text{th}} \end{cases}. \quad (7)$$

Here a corresponds to the relative slope in the normal state [see insert to Fig. 4 b)].

For the case of the 3-pulse experiment one has to calculate the difference (1) using (4) and taking (7) with⁷¹ either $U(r, z) = U_{\text{D}}(r, z) + U_{\text{P}}(r, z)$ or $U(r, z) = U_{\text{D}}(r, z)$ leading to:

$$\Delta\epsilon_3(r, z) = \Delta\epsilon_0(h[U(r, z) + U_{\text{P}}(r, z)] - h[U_{\text{D}}(r, z)]). \quad (8)$$

Here we assume that the probe arrives after P and D pulses and neglect any temporal evolution.

For calculation of the diffusive recovery within the framework of the saturation model we neglect the radial dependence and approximate the depth profile with

a Gaussian:

$$U(z, t) = U_0 \exp[-z^2/z_0^2(1+t/\tau_{\text{D}})] / \sqrt{1+t/\tau_{\text{D}}}, \quad (9)$$

where, $z_0 \sim \alpha^{-1}$, corresponds to the optical penetration depth, $\tau_{\text{D}} = z_0^2/4D$, is given by the diffusion constant D and U_0 is the peak energy density.

In the case of an acoustic strain wave propagating perpendicular to the surface³¹ one can approximate $\Delta\epsilon(r, z)$ by a Heaviside function along z ,

$$\Delta\epsilon(r, z) \propto \exp[-2r^2/\rho_{\text{P}}^2] [1 - \text{H}(z - c_{\text{s}}t)], \quad (10)$$

where c_{s} corresponds to the sound group velocity. The oscillating part of the signal (4) is then,

$$\frac{\Delta R_{\text{osc}}}{R} \propto e^{-\alpha c_{\text{s}}t} \cos(4\pi n c_{\text{s}}t/\lambda_{\text{pr}} - \phi), \quad (11)$$

with λ_{pr} being the probe vacuum wavelength. The sound speed is given by,

$$c_{\text{s}} = \lambda_{\text{pr}} \nu_{\text{s}}/2n, \quad (12)$$

where ν_{s} corresponds to the measured coherent oscillation frequency.

* tomaz.mertelj@ijs.si

¹ C. Berthier, P. Molinié, and D. Jérôme, *Solid State Communications* **18**, 1393 (1976).

² A. F. Kusmartseva, B. Sipos, H. Berger, L. Forró, and E. Tutiš, *Physical Review Letters* **103**, 236401 (2009).

³ B. Sipos, A. F. Kusmartseva, A. Akrap, H. Berger, L. Forró, and E. Tutiš, *Nature Materials* **7**, 960 (2008).

⁴ S. Gao, F. Flicker, R. Sankar, H. Zhao, Z. Ren, B. Rachmilowitz, S. Balachandar, F. Chou, K. S. Burch, Z. Wang, J. van Wezel, and I. Zeljkovic, *Proceedings of the National Academy of Sciences* **115**, 6986 (2018).

⁵ T. Qian, M. H. Christensen, C. Hu, A. Saha, B. M. Andersen, R. M. Fernandes, T. Birol, and N. Ni, *Physical Review B* **104**, 144506 (2021).

⁶ S. Qiao, X. Li, N. Wang, W. Ruan, C. Ye, P. Cai, Z. Hao, H. Yao, X. Chen, J. Wu, Y. Wang, and Z. Liu, *Physical Review X* **7** (2017), 10.1103/PhysRevX.7.041054.

⁷ Y. Yu, F. Yang, X. F. Lu, Y. J. Yan, Y.-H. Cho, L. Ma, X. Niu, S. Kim, Y.-W. Son, D. Feng, S. Li, S.-W. Cheong, X. H. Chen, and Y. Zhang, *Nature Nanotechnology* **10**, 270 (2015).

⁸ U. Chatterjee, J. Zhao, M. Iavarone, R. Di Capua, J. P. Castellán, G. Karapetrov, C. D. Malliakas, M. G. Kanatzidis, H. Claus, J. P. C. Ruff, F. Weber, J. van Wezel, J. C. Campuzano, R. Osborn, M. Randeria, N. Trivedi, M. R. Norman, and S. Rosenkranz, *Nature Communications* **6**, 6313 (2015).

⁹ S. F. Meyer, R. E. Howard, G. R. Stewart, J. V. Acrivos, and T. H. Geballe, *The Journal of Chemical Physics* **62**, 4411 (1975).

¹⁰ E. Morosan, H. W. Zandbergen, B. S. Dennis, J. W. G.

Bos, Y. Onose, T. Klimczuk, A. P. Ramirez, N. P. Ong, and R. J. Cava, *Nature Physics* **2**, 544 (2006).

¹¹ L. Stojchevska, I. Vaskivskiy, T. Mertelj, P. Kusar, D. Svetin, S. Brazovskii, and D. Mihailovic, *Science (New York, N.Y.)* **344**, 177 (2014).

¹² A. Mraz, R. Venturini, D. Svetin, V. Sever, I. A. Mihailovic, I. Vaskivskiy, B. Ambrozic, G. Dražić, M. D'Antuono, D. Stornaiuolo, F. Tafuri, D. Kazazis, J. Ravnik, Y. Ekinci, and D. Mihailovic, *Nano Letters* **22**, 4814 (2022).

¹³ I. Vaskivskiy, I. A. Mihailovic, S. Brazovskii, J. Gosparic, T. Mertelj, D. Svetin, P. Sutar, and D. Mihailovic, *Nature Communications* **7**, 11442 (2016).

¹⁴ M. Yoshida, R. Suzuki, Y. Zhang, M. Nakano, and Y. Iwasa, *Science Advances* **1**, e1500606 (2015).

¹⁵ D. E. Moncton, J. D. Axe, and F. J. DiSalvo, *Physical Review Letters* **34**, 734 (1975).

¹⁶ D. J. Rahn, S. Hellmann, M. Kalläne, C. Sohrt, T. K. Kim, L. Kipp, and K. Rossnagel, *Physical Review B* **85**, 224532 (2012).

¹⁷ K. Mogami, S. Ohta, and H. Sakata, *Surface Science* **707**, 121636 (2021).

¹⁸ F. Bischoff, W. Auwärter, J. V. Barth, A. Schiffrin, M. Fuhrer, and B. Weber, *Chemistry of Materials* **29**, 9907 (2017).

¹⁹ Y. Liu, R. Ang, W. J. Lu, W. H. Song, L. J. Li, and Y. P. Sun, *Applied Physics Letters* **102**, 192602 (2013).

²⁰ P. B. Littlewood and C. M. Varma, *Physical Review B* **26**, 4883 (1982).

²¹ D. Pekker and C. Varma, *Annual Review of Condensed Matter Physics* **6**, 269 (2015).

- ²² R. Grasset, T. Cea, Y. Gallais, M. Cazayous, A. Sacuto, L. Cario, L. Benfatto, and M.-A. Méasson, *Physical Review B* **97**, 094502 (2018).
- ²³ M.-A. Méasson, Y. Gallais, M. Cazayous, B. Clair, P. Rodière, L. Cario, and A. Sacuto, *Physical Review B* **89**, 060503 (2014).
- ²⁴ R. Sooryakumar and M. V. Klein, *Physical Review Letters* **45**, 660 (1980).
- ²⁵ A. Anikin, R. D. Schaller, G. P. Wiederrecht, E. R. Margine, I. I. Mazin, and G. Karapetrov, *Physical Review B* **102**, 205139 (2020).
- ²⁶ D. T. Payne, P. Barone, L. Benfatto, F. Parmigiani, and F. Cilento, “Lattice contribution to the unconventional charge density wave transition in BiFeSe_2 in a non-equilibrium optical approach,” (2020), arXiv:2010.09826 [cond-mat].
- ²⁷ R. Yusupov, T. Mertelj, V. V. Kabanov, S. Brazovskii, P. Kusar, J.-H. Chu, I. R. Fisher, and D. Mihailovic, *Nature Physics* **6**, 681 (2010).
- ²⁸ M. Naseska, A. Pogrebna, G. Cao, Z. Xu, D. Mihailovic, and T. Mertelj, *Physical Review B* **98**, 035148 (2018).
- ²⁹ L. Stojchevska, P. Kusar, T. Mertelj, V. Kabanov, Y. Toda, X. Yao, and D. Mihailovic, *Physical Review B* **84**, 180507 (2011).
- ³⁰ In the 3-pulse experiment the D pulse is not-chopped and therefore its contribution to the Pr is suppressed [see Eq. (1)].
- ³¹ C. Thomsen, H. T. Grahn, H. J. Maris, and J. Tauc, *Optics Communications* **60**, 55 (1986).
- ³² S. V. Dordevic, D. N. Basov, R. C. Dynes, and E. Bucher, *Physical Review B* **64**, 161103 (2001).
- ³³ The error bar is the non-linear least square fit error and does not take into account the index of refraction error.
- ³⁴ J. L. Feldman, *Journal of Physics and Chemistry of Solids* **37**, 1141 (1976).
- ³⁵ E. E. Krasovskii, W. Schattke, V. N. Strocov, and R. Claessen, *Physical Review B* **66**, 235403 (2002).
- ³⁶ In the case of the 3-pulse experiment we define the magnitude as value of the transient reflectivity at $t_{\text{PPR}} \sim 18$ ps [the gray bar in Fig. 3 c)] where a plateau is observed in the presence of the D pulse..
- ³⁷ P. Kusar, V. V. Kabanov, J. Demsar, T. Mertelj, S. Sugai, and D. Mihailovic, *Physical Review Letters* **101**, 227001 (2008).
- ³⁸ At the 1.55 eV Pr photon energy³².
- ³⁹ J. M. E. Harper, T. H. Geballe, and F. J. Di Salvo, *Physics Letters A* **54**, 27 (1975).
- ⁴⁰ B. M. Murphy, H. Requardt, J. Stettner, J. Serrano, M. Krisch, M. Müller, and W. Press, *Physical Review Letters* **95**, 256104 (2005).
- ⁴¹ The CDW gap is concentrated on few hot spots with large amounts of ungapped Fermi surface.^{16,72}
- ⁴² J. Demsar, K. Biljaković, and D. Mihailovic, *Physical Review Letters* **83**, 800 (1999).
- ⁴³ R. Yusupov, T. Mertelj, J.-H. Chu, I. Fisher, and D. Mihailovic, *Physical review letters* **101**, 246402 (2008).
- ⁴⁴ L. Stojchevska, M. Borovšak, P. Foury-Leylekan, J.-P. Pouget, T. Mertelj, and D. Mihailovic, *Physical Review B* **96**, 035429 (2017).
- ⁴⁵ V. Nasretdinova, M. Borovšak, J. Mravlje, P. Šutar, E. Goreshnik, T. Mertelj, and D. Mihailovic, *Physical Review B* **99**, 085101 (2019).
- ⁴⁶ C. N. Kuo, D. Shen, B. S. Li, N. N. Quyen, W. Y. Tzeng, C. W. Luo, L. M. Wang, Y. K. Kuo, and C. S. Lue, *Physical Review B* **99**, 235121 (2019).
- ⁴⁷ A. Mialitsin, *Journal of Physics and Chemistry of Solids Spectroscopy and Optics* **172**, 568 (2015).
- ⁴⁸ J. Demsar, R. D. Averitt, A. J. Taylor, V. V. Kabanov, W. N. Kang, H. J. Kim, E. M. Choi, and S. I. Lee, *Physical Review Letters* **91**, 267002 (2003).
- ⁴⁹ M. Beck, M. Klammer, S. Lang, P. Leiderer, V. V. Kabanov, G. N. Gol’tsman, and J. Demsar, *Physical Review Letters* **107**, 177007 (2011).
- ⁵⁰ T. Akiba, Y. Toda, S. Tsuchiya, M. Oda, T. Kurosawa, D. Mihailovic, and T. Mertelj, submitted to PRB (2023).
- ⁵¹ A. Rothwarf and B. Taylor, *Physical Review Letters* **19**, 27 (1967).
- ⁵² V. V. Kabanov, J. Demsar, and D. Mihailovic, *Physical review letters* **95**, 147002 (2005).
- ⁵³ At strong excitations the saturation non linearity naturally transition in BiFeSe_2 in a non-equilibrium optical approach,”
- ⁵⁴ T. Mertelj, A. Ošlak, J. Dolinšek, I. R. Fisher, V. V. Kabanov, and D. Mihailovic, *Physical Review Letters* **102**, 086405 (2009).
- ⁵⁵ Replacing the first term in brackets with $\exp(-t/\tau)$.
- ⁵⁶ With respect to the probe.
- ⁵⁷ The advanced diffusion model fits virtually overlap the simple diffusion model at 1.55 eV PPE and are not shown.
- ⁵⁸ In the framework of the saturation model.
- ⁵⁹ T. Mertelj, P. Kusar, V. V. Kabanov, P. Giraldo-Gallo, I. R. Fisher, and D. Mihailovic, *Physical Review Letters* **110**, 156401 (2013).
- ⁶⁰ G. Orenstein, R. A. Duncan, G. A. d. I. P. Munoz, Y. Huang, V. Krapivin, Q. L. Nguyen, S. Teitelbaum, A. G. Singh, R. Mankowsky, H. Lemke, M. Sander, Y. Deng, C. Arrell, I. R. Fisher, D. A. Reis, and M. Trigo, “Subdiffusive Dynamics of Topological Vortex Strings of a Charge Density Wave,” (2023), arXiv:2304.00168 [cond-mat].
- ⁶¹ Calculating the T -dependent in-plane equilibrium heat diffusion constant from literature data^{39,73} we obtain $D_{\text{eq-ip}} \sim 1 \text{ cm}^2/\text{s}$ at T_{CDW} increasing with decreasing T to $D_{\text{eq-ip}} \sim 30 \text{ cm}^2/\text{s}$ at T_c .
- ⁶² In the strong excitation cases, D_{op} is found smaller, ~ 0.2 and $\sim 0.01 \text{ cm}^2/\text{s}$ (at $T = 4$ K) for the 1.55 eV PPE and 3.1 eV PPE excitation, respectively. Here, however, one should take into account that the transient T in the strong excitation cases is of the order of T_{CDW} . D_{op} is therefore found ~ 20 times smaller (at $T \sim 26$ K) and ~ 40 times smaller (at $T \sim 48$ K) than $D_{\text{eq-ip}}$ for the 1.55 eV PPE and 3.1 eV PPE excitation, respectively.
- ⁶³ F. Roeske, H. R. Shanks, and D. K. Finnemore, *Physical Review B* **16**, 3929 (1977).
- ⁶⁴ A. LeBlanc and A. Nader, *Solid State Communications* **150**, 1346 (2010).
- ⁶⁵ B. W. Pfalzgraf and H. Spreckels, *Journal of Physics C: Solid State Physics* **20**, 4359 (1987).
- ⁶⁶ H. Schaefer, V. V. Kabanov, and J. Demsar, *Physical Review B* **89**, 045106 (2014).
- ⁶⁷ While the observed transient reflectivity dynamics clearly contains some sub-picosecond-timescale components the CDW component rise time is significantly slower than the AM oscillation period.
- ⁶⁸ Anikin *et al.*²⁵ observed a ~ 4 -THz ($\sim 130 \text{ cm}^{-1}$) coherent mode at 2.2 eV PPE, which softens by $\sim 10\%$ with increasing T towards T_{CDW} . The data were, however, taken at rather high $F_P = 250 \mu\text{J}/\text{cm}^2$, well above the CDW destruction threshold fluence, F_{th} , and the mode persists in the normal state so it cannot correspond to the back-folded lattice mode contributing to the CDW OP.
- ⁶⁹ At comparable volume excitation densities.
- ⁷⁰ While both Nader *et al.* and Trigo *et al.* (2010, 2015) and

ing wavelengths.

⁷¹ Here we implicitly assume a chosen and fixed t_{DP} .

⁷² S. V. Borisenko, A. A. Kordyuk, V. B. Zabolotnyy, D. S. Inosov, D. Evtushinsky, B. Büchner, A. N. Yaresko,

A. Varykhalov, R. Follath, W. Eberhardt, L. Patthey, and H. Berger, *Physical Review Letters* **102**, 166402 (2009).

⁷³ V. I. Beletskii, O. A. Gavrenko, B. A. Merisov, M. A. Obolenskii, A. V. Sologubenko, G. Y. Khadjai, and K. B. Chashka, *Low Temperature Physics* **24**, 273 (1998).